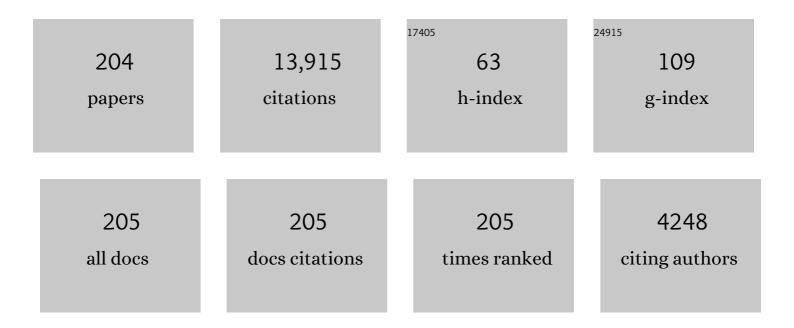
Yong-Cheng Lin

List of Publications by Year in descending order

Source: https://exaly.com/author-pdf/1642494/publications.pdf Version: 2024-02-01



#	Article	IF	CITATIONS
1	A critical review of experimental results and constitutive descriptions for metals and alloys in hot working. Materials & Design, 2011, 32, 1733-1759.	5.1	1,094
2	Constitutive modeling for elevated temperature flow behavior of 42CrMo steel. Computational Materials Science, 2008, 42, 470-477.	1.4	535
3	EBSD study of a hot deformed nickel-based superalloy. Journal of Alloys and Compounds, 2015, 640, 101-113.	2.8	460
4	Dynamic recrystallization behavior of a typical nickel-based superalloy during hot deformation. Materials & Design, 2014, 57, 568-577.	5.1	419
5	A modified Johnson–Cook model for tensile behaviors of typical high-strength alloy steel. Materials Science & Engineering A: Structural Materials: Properties, Microstructure and Processing, 2010, 527, 6980-6986.	2.6	295
6	Prediction of 42CrMo steel flow stress at high temperature and strain rate. Mechanics Research Communications, 2008, 35, 142-150.	1.0	269
7	Application of neural networks to predict the elevated temperature flow behavior of a low alloy steel. Computational Materials Science, 2008, 43, 752-758.	1.4	243
8	Hot deformation behavior and processing map of a typical Ni-based superalloy. Materials Science & Engineering A: Structural Materials: Properties, Microstructure and Processing, 2014, 591, 183-192.	2.6	235
9	Hot deformation and processing map of a typical Al–Zn–Mg–Cu alloy. Journal of Alloys and Compounds, 2013, 550, 438-445.	2.8	230
10	Constitutive descriptions for hot compressed 2124-T851 aluminum alloy over a wide range of temperature and strain rate. Computational Materials Science, 2010, 50, 227-233.	1.4	226
11	A physically-based constitutive model for a typical nickel-based superalloy. Computational Materials Science, 2014, 83, 282-289.	1.4	217
12	EBSD analysis of evolution of dynamic recrystallization grains and δ phase in a nickel-based superalloy during hot compressive deformation. Materials and Design, 2016, 97, 13-24.	3.3	217
13	Moisture sorption–desorption–resorption characteristics and its effect on the mechanical behavior of the epoxy system. Polymer, 2005, 46, 11994-12003.	1.8	194
14	Effect of temperature and strain rate on the compressive deformation behavior of 42CrMo steel. Journal of Materials Processing Technology, 2008, 205, 308-315.	3.1	173
15	Constitutive models for high-temperature flow behaviors of a Ni-based superalloy. Materials & Design, 2014, 59, 115-123.	5.1	163
16	The kinetics of dynamic recrystallization of 42CrMo steel. Materials Science & Engineering A: Structural Materials: Properties, Microstructure and Processing, 2012, 556, 260-266.	2.6	156
17	Hot tensile deformation behaviors and fracture characteristics of a typical Ni-based superalloy. Materials & Design, 2014, 55, 949-957.	5.1	154
18	Hot tensile deformation and fracture behaviors of AZ31 magnesium alloy. Materials & Design, 2013, 49, 209-219.	5.1	145

#	Article	IF	CITATIONS
19	Microstructural evolution of a nickel-based superalloy during hot deformation. Materials & Design, 2015, 77, 41-49.	5.1	136
20	Work-hardening behaviors of typical solution-treated and aged Ni-based superalloys during hot deformation. Journal of Alloys and Compounds, 2015, 618, 372-379.	2.8	135
21	Hot tensile deformation behaviors and constitutive model of an Al–Zn–Mg–Cu alloy. Materials & Design, 2014, 59, 141-150.	5.1	133
22	A review of the influencing factors on anisotropic conductive adhesives joining technology in electrical applications. Journal of Materials Science, 2008, 43, 3072-3093.	1.7	132
23	Microstructural evolution and constitutive models to predict hot deformation behaviors of a nickel-based superalloy. Vacuum, 2017, 137, 104-114.	1.6	131
24	Study of dynamic recrystallization in a Ni-based superalloy by experiments and cellular automaton model. Materials Science & Engineering A: Structural Materials: Properties, Microstructure and Processing, 2015, 626, 432-440.	2.6	129
25	Precipitation hardening of 2024-T3 aluminum alloy during creep aging. Materials Science & Engineering A: Structural Materials: Properties, Microstructure and Processing, 2013, 565, 420-429.	2.6	128
26	Effects of initial δ phase on hot tensile deformation behaviors and fracture characteristics of a typical Ni-based superalloy. Materials Science & Engineering A: Structural Materials: Properties, Microstructure and Processing, 2014, 598, 251-262.	2.6	127
27	Low cycle fatigue and creep-fatigue interaction behavior of nickel-base superalloy CH4169 at elevated temperature of 650 °C. Materials Science & Engineering A: Structural Materials: Properties, Microstructure and Processing, 2016, 655, 175-182.	2.6	124
28	A combined Johnson–Cook and Zerilli–Armstrong model for hot compressed typical high-strength alloy steel. Computational Materials Science, 2010, 49, 628-633.	1.4	123
29	A phenomenological constitutive model for high temperature flow stress prediction of Al–Cu–Mg alloy. Materials Science & Engineering A: Structural Materials: Properties, Microstructure and Processing, 2012, 534, 654-662.	2.6	119
30	Microstructural evolution and support vector regression model for an aged Ni-based superalloy during two-stage hot forming with stepped strain rates. Materials and Design, 2018, 154, 51-62.	3.3	116
31	A new dynamic recrystallization kinetics model for a Nb containing Ni-Fe-Cr-base superalloy considering influences of initial δphase. Vacuum, 2017, 141, 316-327.	1.6	112
32	Phase transformation and dynamic recrystallization behaviors in a Ti55511 titanium alloy during hot compression. Journal of Alloys and Compounds, 2019, 795, 471-482.	2.8	112
33	Investigation of uniaxial low-cycle fatigue failure behavior of hot-rolled AZ91 magnesium alloy. International Journal of Fatigue, 2013, 48, 122-132.	2.8	111
34	Study of static recrystallization kinetics in a low alloy steel. Computational Materials Science, 2008, 44, 316-321.	1.4	105
35	New constitutive model for high-temperature deformation behavior of inconel 718 superalloy. Materials & Design, 2015, 74, 108-118.	5.1	104
36	Effects of initial aging time on processing map and microstructures of a nickel-based superalloy. Materials Science & Engineering A: Structural Materials: Properties, Microstructure and Processing, 2015, 620, 319-332.	2.6	104

#	Article	IF	CITATIONS
37	EBSD study of grain growth behavior and annealing twin evolution after full recrystallization in a nickel-based superalloy. Journal of Alloys and Compounds, 2017, 724, 198-207.	2.8	104
38	Hot compressive deformation behavior of 7075 Al alloy under elevated temperature. Journal of Materials Science, 2012, 47, 1306-1318.	1.7	103
39	Effects of pre-treatments on aging precipitates and corrosion resistance of a creep-aged Al–Zn–Mg–Cu alloy. Materials and Design, 2015, 83, 866-875.	3.3	103
40	Uniaxial ratcheting and fatigue failure behaviors of hot-rolled AZ31B magnesium alloy under asymmetrical cyclic stress-controlled loadings. Materials Science & Engineering A: Structural Materials: Properties, Microstructure and Processing, 2013, 573, 234-244.	2.6	101
41	Effects of initial microstructures on hot tensile deformation behaviors and fracture characteristics of Ti-6Al-4V alloy. Materials Science & Engineering A: Structural Materials: Properties, Microstructure and Processing, 2018, 711, 293-302.	2.6	101
42	Investigation of moisture diffusion in epoxy system: Experiments and molecular dynamics simulations. Chemical Physics Letters, 2005, 412, 322-326.	1.2	100
43	Microstructural evolution in 42CrMo steel during compression at elevated temperatures. Materials Letters, 2008, 62, 2132-2135.	1.3	100
44	Numerical simulation for stress/strain distribution and microstructural evolution in 42CrMo steel during hot upsetting process. Computational Materials Science, 2008, 43, 1117-1122.	1.4	98
45	A new mathematical model for predicting flow stress of typical high-strength alloy steel at elevated high temperature. Computational Materials Science, 2010, 48, 54-58.	1.4	98
46	Uniaxial ratcheting and low-cycle fatigue failure behaviors of AZ91D magnesium alloy under cyclic tension deformation. Journal of Alloys and Compounds, 2011, 509, 6838-6843.	2.8	93
47	Effects of hygrothermal aging on epoxy-based anisotropic conductive film. Materials Letters, 2006, 60, 2958-2963.	1.3	91
48	Phase transformation and constitutive models of a hot compressed TC18 titanium alloy in the $\hat{l}\pm+\hat{l}^2$ regime. Vacuum, 2018, 157, 83-91.	1.6	90
49	Study of metadynamic recrystallization behaviors in a low alloy steel. Journal of Materials Processing Technology, 2009, 209, 2477-2482.	3.1	87
50	Effect of creep-aging on precipitates of 7075 aluminum alloy. Materials Science & Engineering A: Structural Materials: Properties, Microstructure and Processing, 2013, 588, 347-356.	2.6	83
51	Study of static recrystallization behavior in hot deformed Ni-based superalloy using cellular automaton model. Materials and Design, 2016, 99, 107-114.	3.3	83
52	Effects of deformation temperatures on stress/strain distribution and microstructural evolution of deformed 42CrMo steel. Materials & Design, 2009, 30, 908-913.	5.1	82
53	Dislocation substructures evolution and an adaptive-network-based fuzzy inference system model for constitutive behavior of a Ni-based superalloy during hot deformation. Journal of Alloys and Compounds, 2017, 708, 938-946.	2.8	79
54	Dynamic softening mechanism in Ti-13V-11Cr-3Al beta Ti alloy during hot compressive deformation. Materials Science & Engineering A: Structural Materials: Properties, Microstructure and Processing, 2016, 665, 154-160.	2.6	76

#	Article	IF	CITATIONS
55	A unified physically based constitutive model for describing strain hardening effect and dynamic recovery behavior of a Ni-based superalloy. Journal of Materials Research, 2015, 30, 3784-3794.	1.2	74
56	2D cellular automaton simulation of hot deformation behavior in a Ni-based superalloy under varying thermal-mechanical conditions. Materials Science & Engineering A: Structural Materials: Properties, Microstructure and Processing, 2017, 691, 88-99.	2.6	72
57	A Phenomenological Constitutive Model for Describing Thermo-Viscoplastic Behavior of Al-Zn-Mg-Cu Alloy Under Hot Working Condition. Experimental Mechanics, 2012, 52, 993-1002.	1.1	69
58	Uniaxial ratchetting behavior of anisotropic conductive adhesive film under cyclic tension. Polymer Testing, 2011, 30, 8-15.	2.3	68
59	Precipitation in Al–Cu–Mg alloy during creep exposure. Materials Science & Engineering A: Structural Materials: Properties, Microstructure and Processing, 2012, 556, 796-800.	2.6	68
60	Study of microstructural evolution during metadynamic recrystallization in a low-alloy steel. Materials Science & Engineering A: Structural Materials: Properties, Microstructure and Processing, 2009, 501, 229-234.	2.6	66
61	Effect of pre-treatment on hot deformation behavior and processing map of an aged nickel-based superalloy. Journal of Alloys and Compounds, 2015, 649, 1075-1084.	2.8	66
62	A unified constitutive model based on dislocation density for an Al-Zn-Mg-Cu alloy at time-variant hot deformation conditions. Materials Science & Engineering A: Structural Materials: Properties, Microstructure and Processing, 2018, 718, 165-172.	2.6	66
63	A precise BP neural network-based online model predictive control strategy for die forging hydraulic press machine. Neural Computing and Applications, 2018, 29, 585-596.	3.2	66
64	Modeling the high-temperature creep behaviors of 7075 and 2124 aluminum alloys by continuum damage mechanics model. Computational Materials Science, 2013, 73, 72-78.	1.4	65
65	Effects of strain on the workability of a high strength low alloy steel in hot compression. Materials Science & Engineering A: Structural Materials: Properties, Microstructure and Processing, 2009, 523, 139-144.	2.6	62
66	Effects of solution temperature and cooling rate on microstructure and micro-hardness of a hot compressed Ti-6Al-4V alloy. Vacuum, 2019, 159, 191-199.	1.6	62
67	Hot tensile deformation behaviors and constitutive model of 42CrMo steel. Materials & Design, 2014, 53, 349-356.	5.1	61
68	Effects of solution treatment on microstructures and micro-hardness of a Sr-modified Al-Si-Mg alloy. Materials Science & Engineering A: Structural Materials: Properties, Microstructure and Processing, 2018, 725, 530-540.	2.6	61
69	Dissolution mechanisms and kinetics of δphase in an aged Ni-based superalloy in hot deformation process. Materials and Design, 2018, 156, 262-271.	3.3	61
70	A new phenomenological constitutive model for hot tensile deformation behaviors of a typical Al–Cu–Mg alloy. Materials & Design, 2013, 52, 118-127.	5.1	59
71	Influences of solution cooling on microstructures, mechanical properties and hot corrosion resistance of a nickel-based superalloy. Materials Science & Engineering A: Structural Materials: Properties, Microstructure and Processing, 2019, 746, 372-383.	2.6	59
72	A dislocation density-based model and processing maps of Ti-55511 alloy with bimodal microstructures during hot compression in α+β region. Materials Science & Engineering A: Structural Materials: Properties, Microstructure and Processing, 2020, 790, 139692.	2.6	59

#	Article	IF	CITATIONS
73	Effects of pre-treatments on mechanical properties and fracture mechanism of a nickel-based superalloy. Materials Science & Engineering A: Structural Materials: Properties, Microstructure and Processing, 2017, 679, 401-409.	2.6	58
74	Microstructural evolution and high temperature flow behaviors of a homogenized Sr-modified Al-Si-Mg alloy. Journal of Alloys and Compounds, 2018, 739, 590-599.	2.8	58
75	Numerical simulation and experimental verification of void evolution inside large forgings during hot working. International Journal of Plasticity, 2013, 49, 53-70.	4.1	56
76	A novel unified dislocation density-based model for hot deformation behavior of a nickel-based superalloy under dynamic recrystallization conditions. Applied Physics A: Materials Science and Processing, 2016, 122, 1.	1.1	56
77	Modeling and simulation of dynamic recrystallization behavior for 42CrMo steel by an extended cellular automaton method. Vacuum, 2017, 146, 142-151.	1.6	56
78	Hot deformation characteristics and dislocation substructure evolution of a nickel-base alloy considering effects of δ phase. Journal of Alloys and Compounds, 2018, 764, 1008-1020.	2.8	56
79	Isothermal tensile deformation behaviors and fracture mechanism of Ti-5Al-5Mo-5V-1Cr-1Fe alloy in β phase field. Vacuum, 2018, 156, 187-197.	1.6	56
80	Study of microstructural evolution during static recrystallization in a low alloy steel. Journal of Materials Science, 2009, 44, 835-842.	1.7	54
81	A new method to predict the metadynamic recrystallization behavior in 2124 aluminum alloy. Computational Materials Science, 2011, 50, 2038-2043.	1.4	54
82	Microstructure evolution and a unified constitutive model for a Ti-55511 alloy deformed in β region. Journal of Alloys and Compounds, 2021, 870, 159534.	2.8	54
83	Evolution of precipitates during two-stage stress-aging of an Al-Zn-Mg-Cu alloy. Journal of Alloys and Compounds, 2016, 684, 177-187.	2.8	53
84	Microstructural variations and kinetic behaviors during metadynamic recrystallization in a nickel base superalloy with pre-precipitated \hat{I}' phase. Materials and Design, 2019, 165, 107584.	3.3	53
85	Spheroidization and dynamic recrystallization mechanisms of Ti-55511 alloy with bimodal microstructures during hot compression in α+β region. Materials Science & Engineering A: Structural Materials: Properties, Microstructure and Processing, 2020, 782, 139282.	2.6	53
86	Kinetics equations and microstructural evolution during metadynamic recrystallization in a nickel-based superalloy with δ phase. Journal of Alloys and Compounds, 2017, 690, 971-978.	2.8	52
87	Effects of annealing parameters on microstructural evolution of a typical nickel-based superalloy during annealing treatment. Materials Characterization, 2018, 141, 212-222.	1.9	52
88	A novel constitutive model for hot deformation behaviors of Ti–6Al–4V alloy based on probabilistic method. Applied Physics A: Materials Science and Processing, 2016, 122, 1.	1.1	50
89	Hot compressive deformation behavior and microstructure evolution of a Ti-55511 alloy with basket-weave microstructures. Vacuum, 2019, 169, 108878.	1.6	50
90	Hot tensile properties, microstructure evolution and fracture mechanisms of Ti-6Al-4V alloy with initial coarse equiaxed phases. Materials Characterization, 2020, 163, 110272.	1.9	50

#	Article	IF	CITATIONS
91	Low-cycle fatigue behaviors of hot-rolled AZ91 magnesium alloy under asymmetrical stress-controlled cyclic loadings. Journal of Alloys and Compounds, 2013, 579, 540-548.	2.8	49
92	A physically-based model considering dislocation–solute atom dynamic interactions for a nickel-based superalloy at intermediate temperatures. Materials and Design, 2019, 183, 108122.	3.3	49
93	Stress-based fatigue life prediction models for AZ31B magnesium alloy under single-step and multi-step asymmetric stress-controlled cyclic loadings. Computational Materials Science, 2013, 73, 128-138.	1.4	48
94	Modeling the creep behavior of 2024-T3 Al alloy. Computational Materials Science, 2013, 67, 243-248.	1.4	48
95	Effect of creep-aging processing on corrosion resistance of an Al–Zn–Mg–Cu alloy. Materials & Design, 2014, 61, 228-238.	5.1	48
96	A comparative study on phenomenon and deep belief network models for hot deformation behavior of an Al–Zn–Mg–Cu alloy. Applied Physics A: Materials Science and Processing, 2017, 123, 1.	1.1	47
97	Microstructural evolution of a Ni-Fe-Cr-base superalloy during non-isothermal two-stage hot deformation. Vacuum, 2018, 151, 283-293.	1.6	47
98	Effects of two-stage creep-aging on precipitates of an Al–Cu–Mg alloy. Materials Science & Engineering A: Structural Materials: Properties, Microstructure and Processing, 2014, 614, 45-53.	2.6	45
99	Effects of creep-aging processing on the corrosion resistance and mechanical properties of an Al–Cu–Mg alloy. Materials Science & Engineering A: Structural Materials: Properties, Microstructure and Processing, 2014, 605, 192-202.	2.6	45
100	Microstructural evolution and grain refinement mechanisms of a Ni-based superalloy during a two-stage annealing treatment. Materials Characterization, 2019, 151, 445-456.	1.9	44
101	Influences of pre-precipitated \hat{l}' phase on microstructures and hot compressive deformation features of a nickel-based superalloy. Vacuum, 2019, 161, 242-250.	1.6	44
102	High-temperature creep behavior of Al–Cu–Mg alloy. Materials Science & Engineering A: Structural Materials: Properties, Microstructure and Processing, 2012, 550, 125-130.	2.6	43
103	Hot deformation behavior of a Sr-modified Al-Si-Mg alloy: Constitutive model and processing maps. Transactions of Nonferrous Metals Society of China, 2018, 28, 592-603.	1.7	42
104	Precipitation behaviors and orientation evolution mechanisms of \hat{I}_{\pm} phases in Ti-55511 titanium alloy during heat treatment and subsequent hot deformation. Materials Characterization, 2020, 167, 110471.	1.9	42
105	A unified dislocation density-based model for an aged polycrystalline Ni-based superalloy considering the coupled effects of complicate deformation mechanisms and initial I´ phase. Materials Science & Engineering A: Structural Materials: Properties, Microstructure and Processing, 2021, 827, 142062.	2.6	40
106	Methods and mechanisms for uniformly refining deformed mixed and coarse grains inside a solution-treated Ni-based superalloy by two-stage heat treatment. Journal of Materials Science and Technology, 2021, 77, 47-57.	5.6	39
107	Effects of pressure on anisotropic elastic properties and minimum thermal conductivity of D022-Ni3Nb phase: First-principles calculations. Journal of Alloys and Compounds, 2016, 688, 285-293.	2.8	38
108	Effects of initial microstructures on serrated flow features and fracture mechanisms of a nickel-based superalloy. Materials Characterization, 2018, 144, 9-21.	1.9	38

#	Article	IF	CITATIONS
109	Hot Tensile Deformation Mechanism and Dynamic Softening Behavior of Ti–6Al–4V Alloy with Thick Lamellar Microstructures. Advanced Engineering Materials, 2020, 22, 1901193.	1.6	38
110	A new method to predict the metadynamic recrystallization behavior in a typical nickel-based superalloy. Applied Physics A: Materials Science and Processing, 2016, 122, 1.	1.1	37
111	Investigation of the effect of hygrothermal conditions on epoxy system by fractography and computer simulation. Materials Letters, 2005, 59, 3831-3836.	1.3	36
112	Prediction of metadynamic softening in a multi-pass hot deformed low alloy steel using artificial neural network. Journal of Materials Science, 2008, 43, 5508-5515.	1.7	36
113	Corrosion resistance of a two-stage stress-aged Al–Cu–Mg alloy: Effects of stress-aging temperature. Journal of Alloys and Compounds, 2016, 657, 855-865.	2.8	36
114	New Constitutive Model for Hot Deformation Behaviors of Ni-Based Superalloy Considering the Effects of Initial δPhase. Journal of Materials Engineering and Performance, 2015, 24, 3527-3538.	1.2	35
115	Investigation on strain dependence of metadynamic recrystallization behaviors of CH4169 superalloy. Vacuum, 2018, 149, 1-11.	1.6	35
116	Precipitation behavior of a Î ² -quenched Ti-5Al-5Mo-5V-1Cr-1Fe alloy during high-temperature compression. Materials Characterization, 2019, 151, 358-367.	1.9	34
117	A strategy to control microstructures of a Ni-based superalloy during hot forging based on particle swarm optimization algorithm. Advances in Manufacturing, 2019, 7, 238-247.	3.2	33
118	Investigation of the Moisture-Desorption Characteristics of Epoxy Resin. Journal of Polymer Research, 2007, 13, 369-374.	1.2	32
119	Improved dislocation density-based models for describing hot deformation behaviors of a Ni-based superalloy. Journal of Materials Research, 2016, 31, 2415-2429.	1.2	32
120	Microstructure Characteristics and Comparative Analysis of Constitutive Models for Flow Stress Prediction of Inconel 718 Alloy. Journal of Materials Engineering and Performance, 2019, 28, 3320-3331.	1.2	32
121	Effects of deformation parameters and stress triaxiality on the fracture behaviors and microstructural evolution of an Al-Zn-Mg-Cu alloy. Journal of Alloys and Compounds, 2020, 832, 154988.	2.8	32
122	Effects of hygrothermal aging on anisotropic conductive adhesive joints: experiments and theoretical analysis. Journal of Adhesion Science and Technology, 2006, 20, 1383-1399.	1.4	31
123	Corrosion resistance of a two-stage stress-aged Al–Cu–Mg alloy: Effects of external stress. Journal of Alloys and Compounds, 2016, 661, 221-230.	2.8	31
124	A design framework for optimizing forming processing parameters based on matrix cellular automaton and neural network-based model predictive control methods. Applied Mathematical Modelling, 2019, 76, 918-937.	2.2	31
125	Effects of two-stage creep-aging processing on mechanical properties of an Al–Cu–Mg alloy. Materials & Design, 2015, 79, 127-135.	5.1	30
126	Influences of stress-aging on the precipitation behavior of δ phase (Ni3Nb) in a nickel-based superalloy. Materials and Design, 2021, 197, 109256.	3.3	30

#	Article	IF	CITATIONS
127	An Enhanced Johnson–Cook Model for Hot Compressed A356 Aluminum Alloy. Advanced Engineering Materials, 2021, 23, .	1.6	30
128	Microstructural evolution of an aged Ni-based superalloy under two-stage hot compression with different strain rates. Materials and Design, 2016, 111, 344-352.	3.3	29
129	Effects of creep-aging parameters on aging precipitates of a two-stage creep-aged Al–Zn–Mg–Cu alloy under the extra compressive stress. Journal of Alloys and Compounds, 2018, 743, 448-455.	2.8	28
130	A deep belief network to predict the hot deformation behavior of a Ni-based superalloy. Neural Computing and Applications, 2018, 29, 1015-1023.	3.2	28
131	Effects of Initial <i>δ</i> Phase on Creep Behaviors and Fracture Characteristics of a Nickelâ€Based Superalloy. Advanced Engineering Materials, 2018, 20, 1700820.	1.6	28
132	Precipitation and dissolution behaviors of δ phase inside a deformed nickel-based superalloy during annealing treatment. Applied Physics A: Materials Science and Processing, 2019, 125, 1.	1.1	28
133	Spheroidization and dynamic recrystallization mechanisms of a novel HIPed P/M superalloy during hot deformation. Journal of Alloys and Compounds, 2022, 910, 164909.	2.8	28
134	Formation mechanism of large grains inside annealed microstructure of GH4169 superalloy by cellular automation method. Journal of Materials Science and Technology, 2019, 35, 1403-1411.	5.6	27
135	Microstructure Evolution and a Unified Constitutive Model of Ti-55511 Alloy Compressed at Stepped Strain Rates. Materials, 2021, 14, 6750.	1.3	27
136	Reliability of Anisotropic Conductive Adhesive Joints in Electronic Packaging Applications. Journal of Adhesion Science and Technology, 2008, 22, 1631-1657.	1.4	26
137	Cyclic Plasticity Constitutive Model for Uniaxial Ratcheting Behavior of AZ31B Magnesium Alloy. Journal of Materials Engineering and Performance, 2015, 24, 1820-1833.	1.2	26
138	An improved kinetics model to describe dynamic recrystallization behavior under inconstant deformation conditions. Journal of Materials Research, 2016, 31, 2994-3003.	1.2	26
139	Study on the structural transition and thermal properties of Ni3Nb-D022 phase: First-principles calculation. Materials and Design, 2018, 139, 16-24.	3.3	26
140	Three-Dimensional Crystal Plasticity Finite Element Simulation of Hot Compressive Deformation Behaviors of 7075 Al Alloy. Journal of Materials Engineering and Performance, 2015, 24, 1294-1304.	1.2	25
141	Effects of solutionizing cooling processing on γ″ (Ni3Nb) phase and work hardening characteristics of a Ni-Fe-Cr-base superalloy. Vacuum, 2017, 144, 86-93.	1.6	25
142	A Particle Swarm Optimization-Based Multi-level Processing Parameters Optimization Method for Controlling Microstructures of an Aged Superalloy During Isothermal Forging. Metals and Materials International, 2019, 25, 1246-1257.	1.8	25
143	A New Creep Constitutive Model for 7075 Aluminum Alloy Under Elevated Temperatures. Journal of Materials Engineering and Performance, 2014, 23, 4350-4357.	1.2	24
144	Effects of initial δ phase (Ni3Nb) on hot tensile deformation behaviors and material constants of Ni-based superalloy. Transactions of Nonferrous Metals Society of China, 2016, 26, 107-117.	1.7	23

#	Article	IF	CITATIONS
145	Modeling Dynamic Recrystallization Behavior in a Novel HIPed P/M Superalloy during High-Temperature Deformation. Materials, 2022, 15, 4030.	1.3	23
146	Physical property and failure mechanism of self-piercing riveting joints between foam metal sandwich composite aluminum plate and aluminum alloy. Journal of Materials Research and Technology, 2022, 17, 139-149.	2.6	22
147	Effects of ultrasonic bonding process on polymer-based anisotropic conductive film joints in chip-on-glass assemblies. Polymer Testing, 2011, 30, 318-323.	2.3	21
148	Electrochemical corrosion behaviors of a stress-aged Al–Zn–Mg–Cu alloy. Journal of Materials Research, 2016, 31, 2493-2505.	1.2	21
149	Precipitation of Secondary Phase and Phase Transformation Behavior of a Solutionâ€Treated Ti–6Al–4V Alloy during Highâ€Temperature Aging. Advanced Engineering Materials, 2020, 22, 1901436.	1.6	21
150	High-temperature deformation behavior and recrystallization mechanism of a near beta titanium alloy Ti-55511 in β phase region. Materials Science & Engineering A: Structural Materials: Properties, Microstructure and Processing, 2022, 847, 143335.	2.6	21
151	Constitutive Model and Processing Maps for a Tiâ€55511 Alloy in β Region. Advanced Engineering Materials, 2020, 22, 1900930.	1.6	20
152	Effects of aging on precipitation behavior and mechanical properties of a tensile deformed Al–Cu alloy. Journal of Alloys and Compounds, 2020, 843, 155975.	2.8	20
153	The dynamic responses of lamellar and equiaxed near β-Ti alloys subjected to multi-pass cross rolling. Journal of Materials Science and Technology, 2020, 43, 220-229.	5.6	20
154	Influences of Initial Microstructures on Portevin‣e Chatelier Effect and Mechanical Properties of a Ni–Fe–Cr–Base Superalloy. Advanced Engineering Materials, 2018, 20, 1800234.	1.6	19
155	Deformation Behavior and Precipitation Features in a Stretched Al–Cu Alloy at Intermediate Temperatures. Materials, 2020, 13, 2495.	1.3	19
156	Effects of solution time and cooling rate on microstructures and mechanical properties of 2219 Al alloy for a larger spun thin-wall ellipsoidal head. Journal of Materials Research and Technology, 2020, 9, 3566-3577.	2.6	19
157	Hot deformation behaviors of a solution-treated Ni-based superalloy under constant and changed strain rates. Vacuum, 2018, 155, 531-538.	1.6	18
158	Staggered spinning of thin-walled Hastelloy C-276 cylindrical parts: Numerical simulation and experimental investigation. Thin-Walled Structures, 2019, 140, 466-476.	2.7	18
159	Creep and Creep-rupture Behavior of 2124-T851 Aluminum Alloy. High Temperature Materials and Processes, 2013, 32, 533-540.	0.6	17
160	EBSD Study of Microstructural Evolution in a Nickelâ€Base Superalloy during Twoâ€Pass Hot Compressive Deformation. Advanced Engineering Materials, 2018, 20, 1800129.	1.6	17
161	Prediction of Ductile Fracture Behaviors for 42CrMo Steel at Elevated Temperatures. Journal of Materials Engineering and Performance, 2015, 24, 221-228.	1.2	16
162	Influence of Stressâ€Aging Processing on Precipitates and Mechanical Properties of a 7075 Aluminum Alloy. Advanced Engineering Materials, 2018, 20, 1700583.	1.6	15

#	Article	IF	CITATIONS
163	Creep Characteristics and Fracture Mechanisms of a Niâ€Based Superalloy with δ Phases at Intermediate Temperatures. Advanced Engineering Materials, 2020, 22, 2000144.	1.6	15
164	Annealing Treatment Methods and Mechanisms for Refining Mixed and Coarse Grains in a Solution Treatment Nickelâ€Based Superalloy. Advanced Engineering Materials, 2019, 21, 1900558.	1.6	14
165	Dislocation Density–Based Model and Stacked Autoâ€Encoder Model for Tiâ€55511 Alloy with Basketâ€Weave Microstructures Deformed in α + β Region. Advanced Engineering Materials, 2021, 23, 2001307.	1.6	13
166	Probabilistic fracture failure analysis of nuclear piping containing defects using R6 method. Nuclear Engineering and Design, 2004, 229, 237-246.	0.8	12
167	Ultrasonic bond process for polymer-based anisotropic conductive film joints. Part 2: Application in chip-on-FR4 board assemblies. Polymer Testing, 2011, 30, 449-456.	2.3	12
168	Effects of pre-treatments on precipitate microstructures and creep-rupture behavior of an Al–Zn–Mg–Cu alloy. Journal of Materials Research, 2016, 31, 1286-1295.	1.2	12
169	Effect of initial mixed grain microstructure state of deformed Ni-based superalloy on its refinement behavior during two-stage annealing treatment. Materials Characterization, 2021, 176, 111130.	1.9	12
170	Effects of solution temperature and cooling rate on <i>α</i> phases and mechanical properties of a forged Ti-55511 alloy. Materials Research Express, 2019, 6, 1165h2.	0.8	11
171	Study of Flow Softening Mechanisms of a Nickel-Based Superalloy With Δ Phase. Archives of Metallurgy and Materials, 2016, 61, 1537-1546.	0.6	10
172	Online optimizing hot forming parameters for alloy parts based on action-dependent heuristic dynamic programming. International Journal of Advanced Manufacturing Technology, 2019, 104, 3745-3757.	1.5	10
173	Localised edgeâ€regionâ€based active contour for medical image segmentation. IET Image Processing, 2021, 15, 1567-1582.	1.4	10
174	Effect of cooling recrystallization annealing treatment on properties of an initial aged deformed GH4169 superalloy. Materials Science & Engineering A: Structural Materials: Properties, Microstructure and Processing, 2022, 831, 142232.	2.6	10
175	The nonlinear unloading behavior of a typical Ni-based superalloy during hot deformation: a new elasto-viscoplastic constitutive model. Applied Physics A: Materials Science and Processing, 2016, 122, 1.	1.1	9
176	A New Method to Increase the Spheroidization Rate of Lamellar <i>α</i> Microstructure during Hot Deformation of a Ti–6Al–4V Alloy. Advanced Engineering Materials, 2020, 22, 2000447.	1.6	9
177	An innovative annealing treatment method and its mechanism to refine deformed mixed grains of initial aged GH4169 superalloy. Journal of Alloys and Compounds, 2022, 907, 164325.	2.8	9
178	Influences of feed rate and wall thickness reduction on the microstructures of thin-walled Hastelloy C-276 cylindrical parts during staggered spinning. International Journal of Advanced Manufacturing Technology, 2020, 106, 3809-3821.	1.5	8
179	Marginal-restraint mandrel-free spinning process for thin-walled ellipsoidal heads. Advances in Manufacturing, 2020, 8, 189-203.	3.2	8
180	High-temperature deformation characteristics and constitutive models of Inconel 625 superalloy. Materials Today Communications, 2022, 32, 103855.	0.9	8

#	Article	IF	CITATIONS
181	The nonlinear unloading behavior of a typical Ni-based superalloy during hot deformation: a unified elasto-viscoplastic constitutive model. Applied Physics A: Materials Science and Processing, 2016, 122, 1.	1.1	7
182	Modeling the two-stage creep-aging behaviors of an Al-Cu-Mg alloy. Materials Research Express, 2018, 5, 096514.	0.8	7
183	Stacked Auto-Encoder Network to Predict Tensile Deformation Behavior of a Typical Nickel-Based Superalloy Considering Portevin–Le Chatelier Effects. Metals and Materials International, 2021, 27, 254-261.	1.8	7
184	Evolution of Annealing Twins in a Hot Deformed Nickel-Based Superalloy. Materials, 2022, 15, 7.	1.3	7
185	Dynamic Softening Mechanism and an Improved Unified Constitutive Model for an Al–Cu–Mn–Fe–Zr Alloy during Warm Deformation. Advanced Engineering Materials, 2021, 23, 2100015.	1.6	6
186	Effects of Aging Treatment on Corrosion Behavior of a Tensile Deformed Al-Cu-Mn-Fe-Zr Alloy in 3.5% NaCl Solution. Materials, 2021, 14, 5062.	1.3	6
187	A New Method for Controlling Billet Temperature During Isothermal Die Forging of a Complex Superalloy Casing. Journal of Materials Engineering and Performance, 2015, 24, 3549-3557.	1.2	5
188	Dynamic recrystallization behaviors of typical solution-treated and aged Ni-based superalloy under stepped strain rates. Procedia Engineering, 2017, 207, 2125-2130.	1.2	5
189	Cu/Li Ratio on the Microstructure Evolution and Corrosion Behaviors of Al–xCu–yLi–Mg Alloys. Acta Metallurgica Sinica (English Letters), 2020, 33, 1201-1216.	1.5	5
190	Microstructural Variation and a Physical Mechanism Model for a Ti-55511 Alloy during Double-Stage Hot Deformation with Stepped Strain Rates in the β Region. Materials, 2021, 14, 6371.	1.3	5
191	Effects of Stressâ€Aging Pretreatment on Hot Deformation Behavior and Microstructure Evolution of a Ni–Cr–Nb–Mo–Ti Alloy. Advanced Engineering Materials, 2021, 23, 2100571.	1.6	4
192	Residual-stress relaxation mechanism and model description of 5052H32 Al alloy spun ellipsoidal heads during annealing treatment. Advances in Manufacturing, 0, , 1.	3.2	4
193	Expert system for integrity assessment of piping containing defects. Expert Systems With Applications, 2006, 30, 149-155.	4.4	3
194	A Yield Stress Model for a Solution-Treated Ni-Based Superalloy during Plastic Deformation. High Temperature Materials and Processes, 2018, 37, 849-856.	0.6	3
195	Effects of Deformation Processing Parameters on the Microstructure Evolution and Microhardness of GH4169 Superalloy during Annealing Treatment. Advanced Engineering Materials, 2021, 23, 2100104.	1.6	3
196	Microstructural Evolution and an Improved Dynamic Recrystallization Kinetic Model of a Ni-Cr-Mo Alloy in Hot Deformation. Materials, 2022, 15, 3161.	1.3	3
197	Finite Element Simulation of the Hot Deformation Behavior of AA7075 Using a Coupled Thermo-Mechanical Crystal Plasticity Constitutive Model. Applied Mechanics and Materials, 0, 553, 82-87.	0.2	2
198	Effect of Post-deformation Annealing Treatment on the Microstructural Evolution of a Cold-Worked Corrosion-Resistant Superalloy (CRSA) Steel. Journal of Materials Engineering and Performance, 2018, 27, 1168-1176.	1.2	2

#	Article	IF	CITATIONS
199	Effects of spinning parameters on microstructures of ellipsoidal heads during marginal-restraint mandrel-free spinning. Advances in Manufacturing, 2020, 8, 457-472.	3.2	2
200	Effects of initial \hat{I}' phase on flow behaviors and dynamically recrystallized grain size of a nickel-based superalloy. Advances in Materials and Processing Technologies, 2015, 1, 84-97.	0.8	1
201	The effect of the different teflon films on anisotropic conductive adhesive film (ACF) bonding. , 2008, , .		Ο
202	Effects of stretching processing parameters on the mean elongation ratio and maximum spread ratio of heavy forgings. Journal of Materials Science, 2011, 46, 7536-7544.	1.7	0
203	Asymmetric Cyclic Deformation Behaviors of Hot-Rolled AZ91 Magnesium Alloy in Rolling Direction. Advanced Materials Research, 2013, 712-715, 38-41.	0.3	Ο
204	The positron and mechanical parameters of a cold-worked aluminum alloy (3004) Using PALT, PADBT and HV ^{**} . Journal of the Mechanical Behavior of Materials, 2021, 30, 292-303.	0.7	0